Int. J. Heat Mass Transfer. Vol. 30, No. 1, pp. 175–185, 1987
Printed in Great Britain

0017–9310/87 $3.00 + 0.00
Pergamon Journals Ltd.

Turbulent duct flow with streamwise nonuniform heating at the duct wall

E. M. SPARROW, A. GARCIA and W. CHUCK
Department of Mechanical Engineering, University of Minnesota, Minneapolis, MN 55455, U.S.A.

(*Received* 25 *February* 1986 *and in final form* 1 *May* 1986)

Abstract—A combined experimental and analytical/numerical investigation has been carried out for turbulent flow in a flat, rectangular duct with streamwise nonuniform heating at one of the principal walls. The investigated heating pattern consisted of adiabatic zones periodically inserted between isothermal heated zones. The relative streamwise lengths of the heated zones and the adiabatic zones were varied parametrically, as was the Reynolds number. Heat transfer coefficients were determined at each of the heated zones, both in the thermal entrance region and in the fully developed region. It was found that the presence of the adiabatic zones can give rise to substantial enhancement of the heat transfer coefficients at the heated zones. For a duct of fixed overall length, the use of the adiabatic zones represents a loss in transfer surface area, which brings about a net decrease in the overall rate of heat transfer. The agreement between the numerical and experimental results was typically in the two percent range, an outcome which recommends the numerical model as a tool for studying other nonuniform heating patterns.

INTRODUCTION

TURBULENT duct flows having longitudinally nonuniform heating at the bounding walls are a reality of engineering practice. Commonly, the heating may vary either monotonically in the flow direction or, alternatively, the variation may be approximately spatially periodic. Furthermore, the use of periodically deployed adiabatic zones to interrupt an otherwise uniform heating at the wall has been proposed as a heat transfer enhancement technique. At such an adiabatic zone, the thermal boundary layer created by the upstream heating tends toward greater temperature uniformity. As a result, the flow approaching the next heated patch undergoes a new thermal boundary-layer development which, in turn, creates high heat transfer coefficients.

The foregoing discussion provides background for the three-part investigation of turbulent, nonuniformly heated duct flows to be described here. The problem to be considered is a flat, rectangular duct in which one of the principal walls is subjected to a spatially periodic heating condition where successive heated zones are separated by adiabatic zones, with each heated zone being isothermal. There is no heat transfer at the other bounding walls of the duct. An unheated hydrodynamic development length delivers a fully developed turbulent flow to the heated test section.

In the first part of the research, experiments were performed for various ratios of the lengths of the consecutive adiabatic and heated zones in the periodic heating pattern. If L_{active} and L_{inact} respectively represent the streamwise lengths of a heated zone and an adiabatic zone, the investigated L_{inact}/L_{active} ratios included 0, 0.095, 0.228, 0.457 and 0.762. For each L_{inact}/L_{active} value, the duct Reynolds number was varied between 4000 and 24,000 in six steps. For each heating pattern and each Reynolds number, heat transfer coefficients were measured at each of the heated segments, extending all the way through the thermal entrance region into the thermally developed regime.

The second part of the research consisted of an analytical–numerical attack on the problem for which experiments were described in the preceding paragraph. The work was performed for a parallel-plate channel and for $Re \geqslant 8000$, i.e. the range for which turbulence models are well established. For the numerical solutions, a marching procedure was used which starts at the very beginning of the heated test section and proceeds downstream along the successive heated and unheated zones. The numerically determined heat transfer coefficients will be compared with those from the experiments.

The third part of the work is a performance analysis. The experimental and numerical results showed that the heat transfer coefficients at the heated zones were enhanced by the presence of the adiabatic zones. On the other hand, the presence of the adiabatic zones represents a loss of heat transfer surface area. *A priori*, it is unknown whether the higher heat transfer coefficients compensate for the loss of the transfer surface area. To investigate this issue, overall heat transfer rates were calculated for ducts having a fixed overall length for heating patterns with no adiabatic zones ($L_{inact}/L_{active} = 0$) and with adiabatic zones characterized by $L_{inact}/L_{active} = 0.25$ and 0.5.

A literature search failed to reveal any prior experimental work on turbulent flow in spatially periodically heated ducts. Furthermore, the problem has, as such, not heretofore been solved analytically. It can,

NOMENCLATURE

A	cross-sectional area for fluid flow
A_i	surface area of element i
A^+	generalized van Driest damping factor
D_h	hydraulic diameter
$\mathscr{D}$	mass diffusion coefficient
f	friction factor
H	half height of duct
H^+	dimensionless half height
h_i	heat transfer coefficient at element i
K_i	mass transfer coefficient at element i
k	thermal conductivity
L_{active}	streamwise length of mass (heat) transfer element
L_{inact}	streamwise length of no mass (heat) transfer zone
L_{tot}	overall length of duct
l^+	dimensionless mixing length
$\dot{M}_i$	rate of mass transfer at element i
ΔM_i	change of mass at element i
$\dot{M}_{tot}$	overall rate of mass transfer for duct length L_{tot}
$\dot{M}_{tot,0}$	value of $\dot{M}_{tot}$ in absence of zero mass transfer zones
Nu_i	Nusselt number at element i
Pr	Prandtl number
Pr_t	turbulent Prandtl number
p	static pressure
$\dot{Q}$	volumetric flow rate
Q_i	rate of heat transfer at element i
Re	Reynolds number
Sc	Schmidt number
Sh_i	Sherwood number at element i
T	temperature
T_b	bulk temperature
T_{bi}	bulk temperature at element i
T_0	fluid inlet temperature
T_w	wall temperature
u	streamwise velocity component
$\bar{u}$	mean velocity
u^+	dimensionless velocity
u^*	friction velocity
x	streamwise coordinate
x_i	coordinate at midpoint of element
x_i'	coordinate at upsteam end of element
x_i''	coordinate at downstream end of element
x^+	dimensionless streamwise coordinate
y	transverse coordinate
y^+	dimensionless transverse coordinate.

Greek symbols

α	thermal diffusivity
ε_h	eddy diffusivity for heat
ε_m	eddy diffusivity for momentum
θ	dimensionless temperature
μ	viscosity
ν	kinematic viscosity
$\rho_{nb,i}$	bulk naphthalene vapor density at element i
ρ_{nw}	naphthalene vapor density at subliming surface
τ	duration of data run
τ	shear stress
τ_w	wall shear stress.

in principle, be treated by superposing Graetz-type solutions for the one-sided heated, isothermal-walled duct [1–3]. Recall that the Graetz solution is a series, the first term of which applies far downstream (in the thermally developed region) and each subsequent term enables the solution to progress upstream toward the test section inlet. Solutions of this type generally do not yield accurate results in the neighborhood of the inlet.

If Graetz-type solutions were to be superposed in an attempt to solve the periodic heating problem, the aforementioned inlet-section inaccuracies would be repeated at the initiation of each cycle of the periodic heating pattern. It is for this reason that superposition of Graetz-type solutions was not used here. As previously noted, the present solutions were obtained by a marching procedure which starts at the very beginning of the heated test section, in contrast to the Graetz solution which starts downstream and tries to work backwards toward the inlet.

Performance analyses to evaluate the use of periodic adiabatic zones as an enhancement technique seem not to have been published up till now.

EXPERIMENTS

Experimental apparatus and procedure

In the design of the experiments, cognizance was taken of the need to achieve a sharply defined, abrupt change in the thermal boundary condition between contiguous portions of the duct wall (i.e. the isothermal and adiabatic zones). Owing to the unavailability of perfect thermal insulators, it is virtually impossible to fulfill the adiabatic condition in the near neighborhood of a heated, isothermal zone. On the other hand, the desired boundary conditions can be achieved by analogy by making use of the naphthalene sublimation technique, and this technique was adopted for the present experiments.

The experiments were performed using a horizontal

rectangular duct having cross-sectional dimensions of 13.335×2.667 cm (width × height), with a hydraulic diameter $D_h = 4.445$ cm and a 5:1 aspect ratio. The duct consisted of a hydrodynamic development length, the test section, and a post-test-section length, which were fabricated as a single unit and were, therefore, continuous. These sections had respective streamwise lengths of $40D_h$, $13D_h$, and $11D_h$.

The apparatus was operated in the open-circuit mode and in suction. Air from the temperature-controlled, naphthalene-free laboratory was drawn into the hydrodynamic development section through a sharp-edged inlet. The air traversed the development section and entered the test section, where it received naphthalene vapor due to sublimation at one of the principal walls of the duct. It continued on through the post-test-section length, whose presence avoided abrupt changes in cross section which would have disturbed the flow in the downstream portion of the test section.

At the exit of the rectangular duct, the air passed into a rectangular-to-circular transition piece and then to a flowmeter (a calibrated orifice plate), a control valve and a blower. The blower was situated in a service corridor adjacent to the laboratory, and its naphthalene-enriched, compression-heated discharge was vented outside the building. This placement of the blower and the outside exhaust enhanced the temperature stability of the laboratory and ensured the absence of naphthalene vapor in the air entering the apparatus.

The upstream portion of the test section is shown in a schematic side view in Fig. 1. As seen there, the upper wall of the test section housed the periodically positioned mass transfer elements. Each mass transfer element consisted of a layer of solid naphthalene and an aluminum substrate onto which the naphthalene had been cast. All the mass transfer elements had the same streamwise length L_{active} ($= 3.335$ cm) and a spanwise width equal to the width of the duct cross section. The mass transfer boundary condition at each element is uniform concentration of naphthalene vapor, which corresponds to uniform temperature for the analogous heat transfer problem.

The zones of zero mass transfer, which correspond to adiabatic zones in the heat transfer analog, were created by precisely machined spacer bars of aluminum placed between the mass transfer elements. In a given array, all of the spacers had a common length L_{inact} and a spanwise width equal to the duct width. During the course of the experiments, five different arrays were employed, characterized by $L_{inact}/L_{active} = 0$, 0.095, 0.228, 0.457 and 0.762. Since L_{active} was fixed, the variation of the L_{inact}/L_{active} ratio was achieved by using four different sets of spacer bars in addition to the no-spacer case.

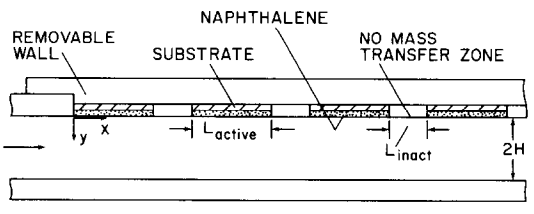

FIG. 1. Upstream portion of test section.

The upper wall of the test section (fabricated from aluminum) was made easily removable to facilitate the rapid installation and extraction of the mass transfer elements and the spacer bars. The elements and spacers, once assembled, were held in place by transverse pressure exerted by longitudinal rails respectively positioned along each lateral edge of the wall. As seen in Fig. 1, the wall was machined at its forward edge with a lip that overlay the adjacent wall of the hydrodynamic development section, and a similar lip was provided at the downstream end of the wall. Sealing against inleakage of air was accomplished by the use of O-ring material which was compressed by the action of quick-connect clamps.

The other walls of the duct were metallic (i.e. aluminum) and, therefore, did not participate in the mass transfer process.

For the casting of the mass transfer elements, each substrate was incorporated into a mold whose surfaces had been hand lapped to a high degree of smoothness. To ensure that the exposed surface of the naphthalene was flush with the surface of the adjacent spacer bar, the spacer bar was incorporated as one wall of the mold. During the casting process, thermocouples were embedded in two of the mass transfer elements such that their junctions were flush with the exposed naphthalene surface.

The freshly cast mass transfer elements, suitably wrapped to suppress sublimation, were placed in the laboratory for at least 12 h to achieve thermal equilibrium. To prepare for a data run, each element was weighed, and the elements and their attached spacer bars were immediately assembled onto the upper wall of the test section. Before the assembled wall was put in place in the test section, a shield was installed which screened the wall from the flow cross section and thereby suppressed sublimation. Then, the airflow was activated, and the readings of the thermocouples embedded in the mass transfer elements were monitored. Once steady state had been attained, the shield was removed, signalling the beginning of the data run proper.

The duration of the run was chosen to limit the sublimation-related recession of the mass transfer surface to 0.0025 cm. During the run, temperatures and pressures were read periodically. At the termination of the run, the upper wall of the test section was disassembled and the mass transfer elements immediately weighed. Then, without interruption, a calibration procedure was performed to determine the extent of any extraneous mass transfer which might have occurred during the setup and disassembly of

the test section, during the weighing, and during the equilibration period.

The mass measurements were performed with an electronic analytical balance having a resolution of 10^{-5} g. The thermocouples, which had been specifically calibrated, were read to 1 μV, while the orifice-plate pressures were read to 10^{-3} Torr.

Data reduction

The mass transfer coefficient K and the corresponding Sherwood number Sh were evaluated at each of the mass transfer elements which made up the duct wall. At any element i

$$K_i = (\Delta M_i/\tau A_i)/(\rho_{nw} - \rho_{nb,i}), \quad Sh_i = K_i D_h/\mathscr{D}. \quad (1)$$

In the equation for K_i, the quantity ΔM_i is the change of mass of element i due to sublimation at area A_i during the duration τ of the data run. In the denominator, ρ_{nw} and $\rho_{nb,i}$ respectively represent the densities of naphthalene vapor at the subliming surface and in the bulk, both at element i.

Under the assumption of solid–vapor equilibrium at the subliming surface, ρ_{nw} is a function only of the surface temperature. The temperature measurements made during the data runs indicated that temperature uniformity prevailed all along the test section, so that ρ_{nw} was the same at all elements. With the measured surface temperature as input, the naphthalene vapor pressure was evaluated from the vapor pressure–temperature relation for naphthalene [4], after which ρ_{nw} was calculated from the perfect gas law.

With regard to the bulk density $\rho_{nb,i}$, it is relevant to note that the increase of ρ_{nb} due to sublimation at any arbitrary mass transfer element j is

$$(\Delta\rho_{nb})_j = (\Delta M_j/\tau)/\dot{Q} \quad (2)$$

in which $\dot{Q}$ is the volumetric flow rate (virtually a constant along the test section). Then, with equation (2) and with $\rho_{nb} = 0$ at the beginning of the test section, it follows that

$$\rho_{nb,i} = \sum_{j=1}^{i-1} (\Delta\rho_{nb})_j + \tfrac{1}{2}(\Delta\rho_{nb})_i \quad (3)$$

which becomes

$$\rho_{nb,i} = (1/\tau\dot{Q})\left[\sum_{j=1}^{i-1} \Delta M_j + \tfrac{1}{2}\Delta M_i\right] \quad (4)$$

thereby completing the evaluation of K_i.

The mass diffusion coefficient $\mathscr{D}$ appearing in equation (1) was eliminated by making use of the definition of the Schmidt number $Sc = \nu/\mathscr{D}$, where $Sc = 2.5$ for naphthalene diffusion in air [4] and ν is the kinematic viscosity of air.

The Reynolds number was evaluated from the standard definition for duct flows

$$Re = \bar{u}D_h/\nu \quad (5)$$

in which $\bar{u}$ is the mean velocity.

ANALYSIS

The analysis is subdivided into two parts. In the first part, the velocity and eddy diffusivity distributions are solved for. These quantities are used as input to the second part, which deals with the heat/mass transfer problem. The analysis is performed for turbulent flow in a parallel-plate channel of height $2H$, with streamwise and transverse coordinates x, y as shown in Fig. 1. Owing to the presence of the hydrodynamic development section, the velocity distribution in the test section ($x > 0$) is invariant with x.

Velocity problem

Owing to the symmetry of the velocity profile about $y = H$, it is sufficient to solve the velocity problem in only half the channel, $0 \leqslant y \leqslant H$.

The condition of fully developed flow can be expressed as

$$dp/dx = d\tau/dy, \quad \tau = \tau_w[1-(y/H)] \quad (6)$$

where, for turbulent flow,

$$\tau = (\mu+\varepsilon_m)(du/dy). \quad (7)$$

If dimensionless variables are introduced

$$u^+ = u/u^*, \quad y^+ = u^*y/\nu, \quad H^+ = u^*H/\nu \quad (8)$$

$$x^+ = x/H, \quad u^* = (\tau_w/\rho)^{1/2} \quad (9)$$

equations (7)–(9) become

$$(1+\varepsilon_m/\nu)(du^+/dy^+) = 1-(y^+/H^+). \quad (10)$$

The eddy diffusivity for momentum ε_m varies with y^+ in the region adjacent to the channel wall but is virtually constant in the core of the flow (see Fig. 7-63 of [5] and Fig. 2 of [6]). For the core region,

$$\varepsilon_m/\nu = 0.079H^+. \quad (11)$$

Adjacent to the wall, ε_m will be represented by a mixing length—damping factor model

$$\varepsilon_m/\nu = (l^+)^2(du^+/dy^+),$$

$$l^+ = \kappa y^+[1-\exp(-y^+/A^+)] \quad (12)$$

where l^+ is the mixing length, $\kappa = 0.4$ is the von Karman constant, and A^+ is a generalized van Driest damping factor. In ref. [7], an empirical representation is given for A^+ as a function of the dimensionless streamwise pressure gradient dp/dx and the transverse velocity v_w at the wall. For the heat transfer applications of interest here, $v_w = 0$, while in the naphthalene sublimation experiments, $v_w \sim 10^{-5}\bar{u}$ and is, therefore, entirely negligible. Thus, from [7]

$$A^+ = 25/(1+30.175p^+),$$

$$p^+ = \mu(dp/dx)/(\rho\tau_w^3)^{1/2} = -(1/H^+). \quad (13)$$

The boundary between the near-wall and core regions will be derived shortly.

The final forms of the governing equations for the velocity can now be obtained. For the near-wall

region, equations (12) and (13) are introduced into equation (10), and the resulting quadratic is solved for du^+/dy^+

$$du^+/dy^+ = [\![2(1-y^+/H^+)]\!]/ [\![1+[1+4\{\kappa y^+(1-\exp(-y^+/A^+))\}^2 \times(1-y^+/H^+)]^{1/2}]\!]. \quad (14)$$

Note that the near-wall ε_m can be represented as an algebraic function of y^+ by combining equations (12), (13) and (14). The boundary between the near-wall and core regions will be defined as the position $y^+ = Y^+$ at which the near-wall ε_m equals the core ε_m as given by equation (11). By using the aforementioned near-wall algebraic representation for ε_m, there follows

$$0.079H^+ = -\tfrac{1}{2}+\tfrac{1}{2}[1+4\{\kappa Y^+(1-\exp(-Y^+/A^+))\}^2 \times(1-Y^+/H^+)]^{1/2}. \quad (15)$$

This equation can be solved numerically to obtain Y^+. The quantity A^+, which appears as a parameter, is a function of H^+. Consequently, Y^+ can be obtained for parametric values of H^+.

The differential equation (14) can now be solved to find u^+ in the range $0 \leqslant y^+ \leqslant Y^+$ for parametric values of H^+. The solution was obtained numerically via the Runge–Kutta method, subject to the boundary condition $u^+ = 0$ at $y^+ = 0$. From the solution, the computed value of u^+ at $y^+ = Y^+$ may be denoted by U^+.

For the core region, $Y^+ \leqslant y^+ \leqslant H^+$, equation (10) can be integrated directly since ε_m is a constant. This yields

$$u^+ = U^+ + [(y^+ - Y^+) - \{(y^+)^2 - (Y^+)^2\}/2H^+]/(1+0.079H^+). \quad (16)$$

It now remains to relate the parameter H^+ to the Reynolds number. From its definition, the Reynolds number can be evaluated as

$$Re = \bar{u}D_h/\nu = 4\int_0^{H^+} u^+ \, dy^+ \quad (17)$$

where the hydraulic diameter $D_h = 4H$ for a parallel-plate channel. By means of equation (17), the Reynolds number corresponding to each H^+ can be evaluated. In addition, the friction factor f can be related to the Reynolds number via

$$H^+ = (Re/4)(f/8)^{1/2}. \quad (18)$$

The numerically determined friction factors were compared with those from the Jones modification [8] of the Prandtl equation. The Prandtl equation is for turbulent flow in a circular tube, and to generalize it to rectangular ducts, Jones introduced a modified Reynolds number $Re' = \chi Re$ (Re = hydraulic-diameter Reynolds number), where $\chi = 2/3$ for a parallel-plate channel. In terms of Re', the modified Prandtl equation is

$$f^{-1/2} = 2\log(Re' f^{1/2}) - 0.8. \quad (19)$$

The comparison between the present numerical results for f and those of equation (19) was made over the Reynolds number range from 7000 to 40,000. For $Re \geqslant 10{,}000$, agreement was in the 0.5% range; the maximum deviation was 1.5% at $Re = 7000$. This level of agreement lends confidence to the numerically determined velocity profiles.

Heat and mass transfer problems

Owing to the analogy between the two processes, the solutions for heat transfer problems can be used for mass transfer problems and vice versa. Since heat transfer terminology is more familiar than mass transfer terminology, the forthcoming analysis will be made for heat transfer, but the final Nusselt number results will serve equally well as Sherwood number results.

For hydrodynamically developed turbulent flow in a parallel-plate channel, the energy equation can be written as

$$u(\partial T/\partial x) = (\partial/\partial y)[(\alpha+\varepsilon_h)(\partial T/\partial y)] \quad (20)$$

in which ε_h is the eddy diffusivity for heat. To obtain a dimensionless representation of equation (20), the u^+, x^+ and y^+ variables of equations (8) and (9) are used in conjunction with

$$\theta = (T-T_0)/(T_w-T_0), \quad Pr_t = \varepsilon_m/\varepsilon_h \quad (21)$$

so that

$$u^+(\partial\theta/\partial x^+) = H^+(\partial/\partial y^+)[\{1/Pr + (\varepsilon_m/\nu)/Pr_t\}(\partial\theta/\partial y^+)]. \quad (22)$$

In the definition of θ, T_0 is the bulk temperature of the fluid entering the test section and T_w is the temperature of the isothermal zones at the duct wall.

The u^+ and ε_m/ν distributions appearing in equation (22) are already available from the velocity solution. The turbulent Prandtl number Pr_t is commonly taken to be 0.9 or 1. For mass transfer problems, the turbulent Schmidt number is generally set equal to 1. Since the solutions to be obtained here will ultimately be used for comparison with the results of mass transfer experiments, $Pr_t = 1$ will be employed.

The boundary conditions for equation (22) are

$$\theta = 1 \quad \text{at} \quad y^+ = 0 \quad \text{for the isothermal zones} \quad (23)$$

$$\partial\theta/\partial y = 0 \quad \text{at} \quad y^+ = 0 \quad \text{for the adiabatic zones} \quad (24)$$

$$\partial\theta/\partial y = 0 \quad \text{at} \quad y^+ = 2H^+ \quad (25)$$

$$\theta = 0 \quad \text{at} \quad x^+ = 0. \quad (26)$$

The solution of equation (22) was carried out numerically after it was recast in implicit finite-difference form, and the details of the numerical work are available in [9]. Numerical results were obtained for Reynolds numbers of 8000, 11,500, 16,500, and 24,000

and, for each Reynolds number, for heating patterns defined by $L_{inact}/L_{active} = 0$, 0.095, 0.228, 0.457 and 0.762. These parameter values correspond to those of the experiments described earlier in the paper. The Prandtl number appearing in equation (22) was set equal to 2.5 in cognizance of the forthcoming comparisons with the mass transfer experiments, for which $Sc = 2.5$.

Heat transfer coefficients and Nusselt numbers were evaluated from the numerical solutions for each of the isothermal zones. For zone i

$$h_i = Q_i/A_i(T_w - T_{bi}), \quad Nu_i = h_i D_h/k. \tag{27}$$

To implement equation (27), suppose that zone i extends from x_i' to x_i'', with midpoint x_i and surface area A_i (per unit width)

$$x_i = \tfrac{1}{2}(x_i' + x_i''), \quad A_i = x_i'' - x_i'. \tag{28}$$

At any x in the zone, the local heat flux q was evaluated from the finite-difference form of Fourier's Law, after which Q_i was obtained from

$$Q_i = \int_{x_i'}^{x_i''} q\,dx. \tag{29}$$

The bulk temperature T_{bi} was taken to be the average of $T_b(x_i')$ and $T_b(x_i'')$, which corresponds to the practice used in the data reduction for the experiments. At either x_i' and x_i''

$$(T_b - T_0)/(T_w - T_0) = \int_0^{2H} \theta u\,dy \Big/ \int_0^{2H} u\,dy$$

$$= (2/Re)\int_0^{2H^+} \theta u^+\,dy^+. \tag{30}$$

The Nusselt numbers evaluated from the foregoing are precisely equal to Sherwood numbers for $Sc = 2.5$.

RESULTS AND DISCUSSION

Experimental results

The experimentally determined streamwise distributions of the Sherwood number at successive mass transfer elements are presented in Figs. 2–4. In each figure, the per-element Sherwood number, denoted by Sh_i, is plotted as a function of the dimensionless streamwise coordinate x_i/D_h at the centers of the respective elements. Figure 2 conveys results for $Re = 4000$ and 5700, Fig. 3 for $Re = 8000$ and 11,500 and Fig. 4 for $Re = 16{,}500$ and 24,000. For each Reynolds number, Sh_i distributions are plotted for mass transfer patterns characterized by $L_{inact}/L_{active} = 0$, 0.095, 0.228, 0.457 and 0.762.

For convenience, the data for each value of L_{inact}/L_{active} are tied together by dashed lines, but this is not to imply that the Sh_i vs x_i/D_h distributions are continuous. Note that although the ordinates of the various figures cover different ranges, they all belong to the same logarithmic scale. Therefore, a given vertical distance corresponds to the same *percentage* change in Sh_i in all of the figures.

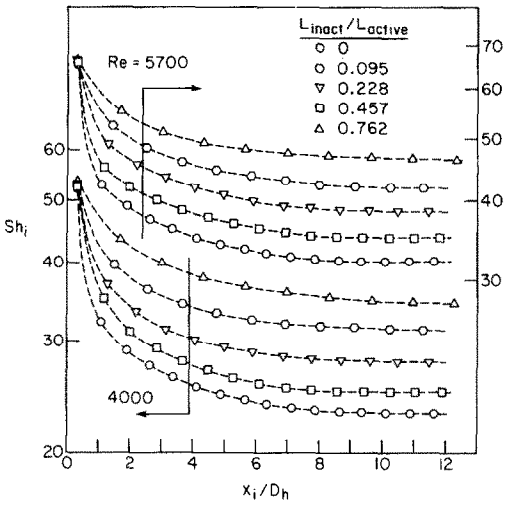

FIG. 2. Experimentally determined per-element Sherwood numbers, $Re = 4000$ and 5700.

An overall examination of Figs. 2–4 reveals that the presence of periodically positioned zones of zero mass transfer enhances the Sherwood number at the mass transfer elements. This is witnessed by the fact that for any given Reynolds number, the Sh_i vs x_i/D_h distributions are arranged one above the other for increasing values of L_{inact}/L_{active}. The extent of the enhancement due to the zero mass transfer zones can be gauged by the vertical separation distance between the distributions. Aside from the neighborhood of the test section inlet, the separation between successive distributions is virtually independent of x_i/D_h. Therefore, representative comparisons can be made at any x_i/D_h away from the inlet.

For example, in the neighborhood of $x_i/D_h = 10$, the Sherwood number for $L_{inact}/L_{active} = 0.762$ is 50%

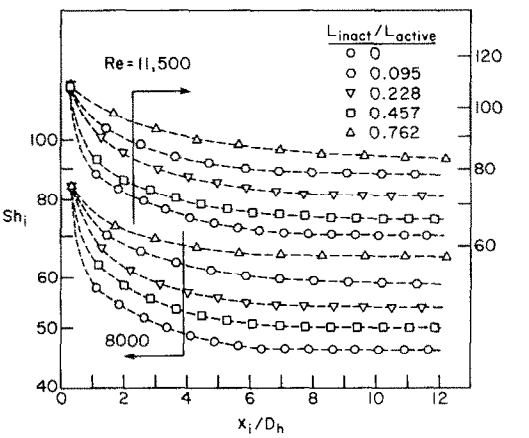

FIG. 3. Experimentally determined per-element Sherwood numbers, $Re = 8000$ and 11,500.

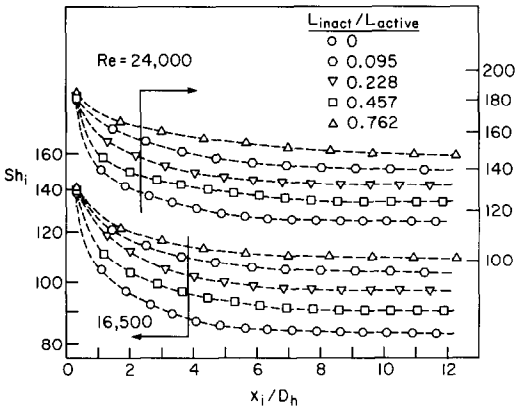

FIG. 4. Experimentally determined per-element Sherwood numbers, Re = 16,500 and 24,000.

greater than that for $L_{inact}/L_{active} = 0$ at $Re = 4000$ and 28% greater at $Re = 24{,}000$. Lesser enhancements occur at smaller values of L_{inact}/L_{active}; e.g. 20% and 14% for $Re = 4000$ and 24,000 when $L_{inact}/L_{active} = 0.228$. These examples demonstrate that by proper choice of the streamwise length of the periodically positioned zones of zero mass transfer, considerable enhancement can be achieved at the mass transfer zones.

Both from inspection of Figs. 2–4 and from the foregoing examples, it is evident that the degree of enhancement for a given value of L_{inact}/L_{active} is substantially greater at low Reynolds numbers than at high Reynolds numbers (note the lesser spread of the Sh_i distributions as Re increases). This behavior is consistent with the well-established fact that low Reynolds number flows are more responsive to factors which alter the temperature and/or velocity fields than are high Reynolds number flows.

From the figures, it is seen that for a given Reynolds number, all of the Sh_i distributions start with a common value (within a 2–3% spread) at the first mass transfer element. Thereafter, with increasing x_i/D_h, there is a monotonic dropoff in Sh_i which becomes progressively more gradual. Ultimately, Sh_i tends toward a fully developed value which is actually achieved for most of the operating conditions investigated here.

Of particular relevance is the fact that the extent of the dropoff, relative to the initial value of Sh_i, becomes progressively smaller as L_{inact}/L_{active} increases. For example, at $Re = 4000$, the dropoff is, respectively, 54 and 36% for $L_{inact}/L_{active} = 0$ and 0.762. The corresponding percentages for $Re = 24{,}000$ are 36 and 20. Thus, the presence of the zones of zero mass transfer lessen the toll that is exacted by the mass transfer entrance region.

The cause of the enhancement associated with the presence of the zero mass tansfer zones has already been set forth in the Introduction. As discussed there, the growth of the mass transfer boundary layer is interrupted and actually reversed as the flow passes over a zero transfer zone. The longer the streamwise length of the zone, the more uniform does the concentration profile become. Furthermore, the more uniform the concentration profile in the flow approaching the next mass transfer element, the higher is the rate of mass transfer at that element. Thus, the results of Figs. 2–4 are physically plausible.

Although the local transfer coefficients are enhanced by the presence of the zero transfer zones, it is uncertain whether the overall rate of transfer from a fixed length of duct will be increased or decreased. This uncertainty arises because the zero mass transfer zones constitute a loss in transfer surface area. The net effect of enhanced local coefficients and reduced surface area will be addressed later.

Numerical–experimental comparison

The experimentally determined per-element Sherwood numbers will be compared in Figs. 5–8 with the predictions of the analytical/numerical model set forth earlier in the paper. Furthermore, to add new perspectives to the results, a format will be used for Figs. 5–8 that differs from that of the preceding figures.

In each of Figs. 5–8, the per-element Sherwood number Sh_i is plotted against the L_{inact}/L_{active} ratio for parametric values of the Reynolds number. Both numerical and experimental results are available and are presented for $Re = 8000$, 11,500, 16,500 and 24,000. For continuity, solid lines have been passed through the numerical results. At the two lower Reynolds numbers, 4000 and 5700, only experimental results are presented because numerical results were not obtained (since the turbulence model applies only to established turbulent flow). The experimental data are interconnected by dashed lines.

Each figure corresponds to a fixed value of x_i/D_h, respectively, 2, 4, 8 and 12. Since the Sh_i at these x_i/D_h were not directly available from either the experimental data or the numerical results, they were obtained by interpolation. In view of the smoothness of the Sh_i vs x_i/D_h distributions (e.g. Figs. 2–4), no

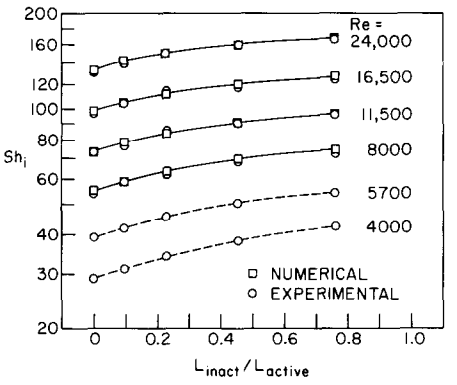

FIG. 5. Comparison of numerically and experimentally determined per-element Sherwood numbers, $x_i/D_h = 2$.

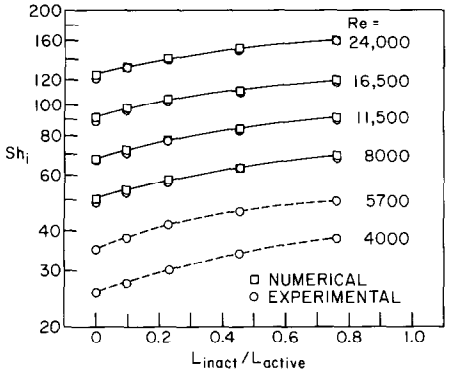

FIG. 6. Comparison of numerically and experimentally determined per-element Sherwood numbers, $x_i/D_h = 4$.

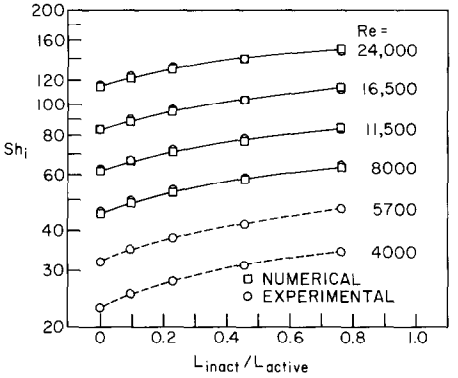

FIG. 8. Comparison of numerically and experimentally determined per-element Sherwood numbers, $x_i/D_h = 12$.

loss of accuracy is expected due to the interpolation. Note that Sh_i is plotted logarithmically in Figs. 5–8, so that a given vertical distance corresponds to the same percentage change regardless of the magnitude of Sh_i.

Attention may first be turned to the comparison of the experimental and numerical results. An overview of Figs. 5–8 indicates a general level of agreement in the 2% range, with an extreme deviation of about 4%. This excellent agreement lends support to both the experimental technique and the numerical model. In particular, it serves to recommend the numerical model as a tool for obtaining results for heating patterns other than those considered here.

The increase of Sh_i with L_{inact}/L_{active} follows a pattern that is common for all cases. In general, for a given Reynolds number, the increase is somewhat more rapid at smaller L_{inact}/L_{active} than at larger L_{inact}/L_{active}. The extent of the increase is greatest at the lowest investigated Reynolds number and diminishes in a regular manner with increasing Reynolds number.

The Sh_i vs L_{inact}/L_{active} distributions display a kind of congruence in that adjacent distributions in any of the figures are virtually equidistant from each other.

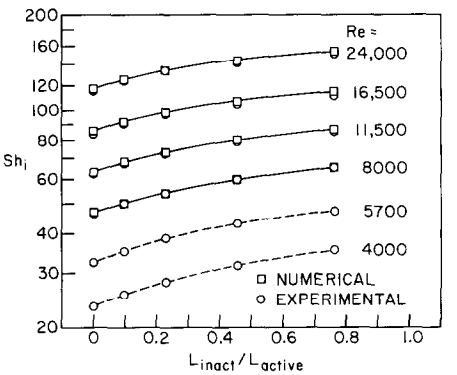

FIG. 7. Comparison of numerically and experimentally determined per-element Sherwood numbers, $x_i/D_h = 8$.

Furthermore, the shapes of the distributions are preserved from one x_i/D_h to another, despite changes in the level of Sh_i. This regularity in the response of Sh_i to L_{inact}/L_{active} means that interpolations of the results to other Reynolds numbers and other x_i/D_h can be performed with high accuracy.

OVERALL PERFORMANCE

It has been demonstrated that the use of periodically positioned zones of zero mass transfer give rise to enhancement at the mass transfer elements, and this finding carries over directly to heat transfer. Depending on the application, this per-element enhancement may be of sufficient value to justify the use of the zero mass transfer zones, regardless of their effect on the overall mass transfer.

In some instances, however, the overall mass transfer (or heat transfer) may be of concern. If the streamwise length of the duct wall is unconstrained, then whatever overall mass transfer is desired can be attained. On the other hand, the situation in which the streamwise length is fixed requires more careful consideration, since the presence of the zero mass transfer zones causes both enhanced transfer coefficients and loss of transfer surface area—effects which are in conflict. The case of the fixed length duct will now be investigated. In particular, the overall rate of mass transfer in the absence of the zero mass transfer zones will be compared with that when the zones are present.

The experiments performed here involved five different test setups, each with a different value of L_{inact}/L_{active}. The overall streamwise lengths of these different test setups were slightly different, so that a comparison of their respective overall rates of mass transfer would not yield the desired fixed-length comparison. To facilitate the fixed-length comparison, a certain amount of computation had to be performed, as will now be described.

The experiments for $L_{inact}/L_{active} = 0$ were per-

formed for an overall length $L_{tot} = 15L_{active}$, and this same value of L_{tot} will be used as the overall length for other configurations where $L_{inact}/L_{active} > 0$. For this L_{tot}, the overall rate of mass transfer will be compared for three cases: $L_{inact}/L_{active} = 0$, 0.25 and 0.50. The comparisons will be made at a common value of the naphthalene vapor density at the subliming surface (corresponding to a temperature of 25°C) and for three different Reynolds numbers.

To begin the analysis, let the rate of mass transfer at any mass transfer element i be denoted as

$$\dot{M}_i = \Delta M_i/\tau \tag{31}$$

so that the overall rate of mass transfer for the length L_{tot} is

$$\dot{M}_{tot} = \sum_{act} \dot{M}_i \tag{32}$$

where the summation includes all the active mass transfer elements contained within the length L_{tot}. From a rearrangement of equation (1), $\dot{M}_i$ can be written as

$$\dot{M}_i/\dot{Q} = [(Sh_i/Sc\,Re)\,(A_i/A)]\,(\rho_{nw} - \rho_{nb,i}) \tag{33}$$

in which all of the symbols have been previously defined, except for A which denotes the fluid-flow cross section of the duct. Furthermore, from equation (4),

$$\rho_{nb,i} = \sum_{j=1}^{i-1} (\dot{M}_j/\dot{Q}) + \tfrac{1}{2}(\dot{M}_i/\dot{Q}). \tag{34}$$

If $\dot{M}_{tot,0}$ is used to represent the overall rate of mass transfer for the $L_{inact}/L_{active} = 0$ case, then for a common Reynolds number (i.e. common volumetric flow $\dot{Q}$),

$$\dot{M}_{tot}/\dot{M}_{tot,0} = (\dot{M}_{tot}/\dot{Q})/(\dot{M}_{tot,0}/\dot{Q}). \tag{35}$$

This equation will be used to compare the $\dot{M}_{tot}$ values corresponding to the presence and the absence of the zero mass transfer zones.

The use of equations (32)–(35) will now be described. As noted earlier, ρ_{nw} was prescribed as the value corresponding to 25°C. Furthermore, $Sc = 2.5$, and A is fixed by the cross-sectional dimensions of the duct. For all cases, A_i (per unit width) = L_{active}. For a given Reynolds number, the Sh_i values needed for equation (33) are directly available in Figs. 2–4 for $L_{inact}/L_{active} = 0$. However, for $L_{inact}/L_{active} = 0.25$ and 0.50, interpolation and crossplotting were used in conjunction with Figs. 2–4 to obtain the Sh_i. In view of the regularity of the data, the resulting Sh_i should be of high accuracy.

In light of the foregoing, all terms on the RHS of equation (33) can be regarded as known except for $\rho_{nb,i}$. By using equations (33) and (34) iteratively, both $\dot{M}_i/\dot{Q}$ and $\rho_{nb,i}$ can be found. To begin the iteration, $\rho_{nb,i}$ is set equal to zero in equation (33) and $\dot{M}_i/\dot{Q}$ is calculated at all of the mass transfer elements. Then, with these values as input, all of the $\rho_{nb,i}$ are evaluated from equation (34). Next, equation (33) is revisited using the updated values of $\rho_{nb,i}$, and new values of $\dot{M}_i/\dot{Q}$ are computed. This procedure is continued to convergence. The converged values of $\dot{M}_i/\dot{Q}$ are used in conjunction with equations (32) and (35) to compare the $\dot{M}_{tot}$ values.

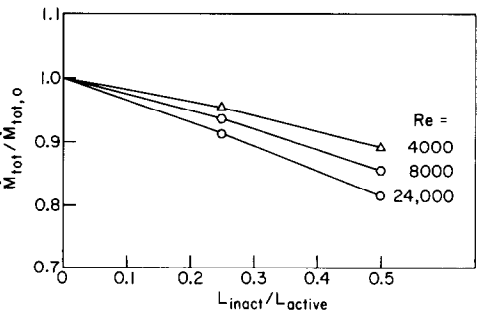

FIG. 9. Effect of no mass transfer zones on the overall rate of mass transfer from a duct of fixed length.

The results of such calculations for $Re = 4000$, 8000 and 24,000 are presented in Fig. 9, where $\dot{M}_{tot}/\dot{M}_{tot,0}$ is plotted against L_{inact}/L_{active} for parametric values of the Reynolds number. As seen in the figure, the overall rate of mass transfer for the fixed-length duct decreases as the length of the zero mass transfer zones increases. The highest transfer rate occurs when there are no zones of zero mass transfer. Thus, in the conflict between higher transfer coefficients at the mass transfer elements and loss of transfer area, both due to the presence of the no mass transfer zones, the latter appears to be the dominant effect.

CONCLUDING REMARKS

This paper has described a combined experimental and analytical/numerical study of turbulent mass (or heat) transfer in a flat, rectangular duct with streamwise-periodic, nonuniform mass (heat) transfer at one of the principal walls. In heat transfer terms, the heating pattern at the wall consisted of adiabatic zones of length L_{inact} periodically inserted between isothermal zones of length L_{active}. The other walls of the duct were adiabatic. Air was delivered to the heated test section by a hydrodynamic development length. In both the experimental and numerical work, heat transfer coefficients were determined at each of the heated elements, extending through the entire thermal entrance region into the thermally developed regime.

The two parameters of the investigation were L_{inact}/L_{active} and the Reynolds number Re. The former was varied between 0 and 0.762 in five steps. For the experiments, the Reynolds number ranged between 4000 and 24,000 in six steps, while the numerical work was confined to $Re \geqslant 8000$, where established turbulence is believed to prevail.

The results of both the experimental and numerical

work indicate that the presence of the periodically positioned adiabatic zones can give rise to substantial enhancement of the heat transfer coefficients at the heated elements, with the greatest relative enhancements occurring at the lower Reynolds numbers. Such localized enhancements may be of sufficient practical value to justify the use of the adiabatic zones regardless of their effect on the overall rate of heat transfer.

With regard to the overall rate of heat transfer, the net effect of the adiabatic zones depends on the overall length of the duct. When the overall length of the duct is fixed, then the presence of the adiabatic zones represents a loss in transfer surface. The conflict between this loss of transfer surface and the enhanced coefficients at the heated elements was examined quantitatively, and it was found that the former wins out. Thus, for a duct of fixed length, the overall rate of heat transfer decreased when the adiabatic zones were present.

The agreement between the numerically and experimentally determined per-element transfer coefficients was typically in the 2% range. This level of agreement serves to recommend the numerical model as a tool for providing results for nonuniform heating patterns other than those considered here.

REFERENCES

1. A. P. Hatton and A. Quarmby, The effect of axially varying and unsymmetrical boundary conditions on heat transfer with turbulent flow between parallel plates, *Int. J. Heat Mass Transfer* **6**, 903–914 (1963).
2. M. Sakakibara and K. Endo, Analysis of heat transfer for turbulent flow between parallel plates, *Int. chem. Engng* **16**, 728–733 (1976).
3. W. M. Kays and M. E. Crawford, *Convective Heat and Mass Transfer*, pp. 265–266. McGraw-Hill, New York (1980).
4. H. H. Sogin, Sublimation from disks to air streams flowing normal to their surfaces, *Trans. Am. Soc. Mech. Engrs* **80**, 61–71 (1958).
5. J. O. Hinze, *Turbulence*, 2nd edn. McGraw-Hill, New York (1975).
6. V. K. Jonsson and E. M. Sparrow, Turbulent diffusivity for momentum transfer in annuli, *J. Basic Engng* **88**, 550–552 (1966).
7. W. M. Kays and M. E. Crawford, *Convective Heat and Mass Transfer*, p. 184. McGraw-Hill, New York (1980).
8. O. C. Jones, Jr., An improvement in the calculation of turbulent friction in rectangular ducts, *J. Fluids Engng* **98**, 173–181 (1976).
9. A. Garcia Gutierrez, Effect of spatially periodic heating or an abrupt contraction at inlet on transitional and turbulent heat transfer in a duct. Ph.D. thesis, Department of Mechanical Engineering, University of Minnesota, Minneapolis, MN (1985).

ECOULEMENT TURBULENT DANS UN CONDUIT AVEC CHAUFFAGE PARIETAL NON UNIFORME DANS LE SENS DU MOUVEMENT

Résumé—Une étude expérimentale et analytique/numérique est conduite pour l'écoulement turbulent dans un canal rectangulaire avec chauffage non uniforme d'une des parois principales. Le cas étudié concerne des zones adiabatiques périodiquement situées entre des zones isothermes chaudes. On fait varier paramétriquement les longueurs relatives des zones alternées, ainsi que le nombre de Reynolds. Les coefficients de transfert sont déterminés à chaque zone chaude, pour la région d'entrée et la région établie. On trouve que la présence des zones adiabatiques peut augmenter sensiblement les coefficients de transfert. Pour un canal de longueur donnée, les zones adiabatiques représentent une perte de surfaces actives au transfert, ce qui mène à une diminution du transfert thermique global. L'accord entre les résultats nnumériques et expérimentaux, de l'ordre de deux pourcent, recommande le modèle numérique pour étudier d'autres configurations de chauffage non uniforme.

TURBULENTE KANALSTRÖMUNG MIT UNGLEICHFÖRMIGER BEHEIZUNG AN DER KANALWAND

Zusammenfassung—Eine kombinierte experimentelle und analytisch/numerische Untersuchung der turbulenten Strömung in einem flachen, rechtwinkligen Kanal mit stellenweise ungleichförmiger Beheizung an einer der Hauptwände wurde durchgeführt. Die untersuchte Meßstrecke bestand aus adiabaten Zonen die periodisch zwischen isotherm beheizten Zonen lagen. Die relative Länge der beheizten Zonen und der adiabaten Zonen wurde, ebenso wie die Reynolds-Zahl, als Parameter geändert. In jeder Heizzone wurden die Wärmeübergangskoeffizienten sowohl im Bereich des thermischen Einlaufs als auch im Bereich der vollausgebildeten Strömung bestimmt. Es wurde festgestellt, daß die Anwesenheit adiabater Zonen Anlaß zu einer erheblichen Verbesserung der Wärmeübergangskoeffizienten in den beheizten Zonen geben kann. Für Kanäle mit vorgegebener Gesamtlänge stellt der Einsatz adiabater Zonen einen Verlust an Wärmeübertragungsfläche dar, der eine Verringerung das übertragenen Nettowärmestroms bringt. Die Abweichung zwischen numerischen und experimentellen Ergebnissen war typisch im Bereich von 2%. Dieses Ergebnis empfiehlt das numerische Modell als Werkzeug für Studien anderer ungleichförmiger Heizmuster.

ТУРБУЛЕНТНОЕ ТЕЧЕНИЕ В КАНАЛЕ С НАГРЕВОМ СТЕНКИ В НАПРАВЛЕНИИ ТЕЧЕНИЯ

Аннотация—Проведено экспериментальное и численно-аналитическое исследование турбулентного течения в плоском прямоугольном канале с неоднородным по течению нагревом одной из его основных стенок. Исследуемая модель состояла из адиабатических зон, периодически размещенных между зонами изотермического нагрева. Относительные длины изотермически и адиабатически нагреваемых зон по течению изменялись параметрически аналогично числу Рейнольдса. Коэффициенты теплоотдачи определялись в каждой из нагреваемых зон в области теплового начального участка при полностью развитом режиме течения. Найдено, что наличие адиабатических зон может привести к существенному увеличению коэффициентов теплоотдачи в зонах нагрева. Использование адиабатических зон в случае канала заданной общей длины дает потерю в площади поверхности нагрева, что ведет к результирующему уменьшению суммарной интенсивности теплообмена. Соответствие между численными и экспериментальными результатами наблюдалось в пределах двух процентов; предложенный численный метод рекомендуется для изучения других режимов неоднородного нагрева.